THE JOURNAL OF PHYSICAL CHEMISTRY C

Article

pubs.acs.org/JPCC

Reduced Bimolecular Charge Recombination Loss in Thermally Annealed Bilayer Heterojunction Photovoltaic Devices with Large External Quantum Efficiency and Fill Factor

Bin Yang, Yongbo Yuan, and Jinsong Huang*

Department of Mechanical and Materials Engineering, and Nebraska Center for Materials and Nanoscience, University of Nebraska−Lincoln, Lincoln, Nebraska 68588-0656, United States

ABSTRACT: Thermally annealed bilayer heterojunction was shown to be an alternative approach to form the bulk-heterojunction (BHJ) structure and yield superior device performance compared to blend-solution-processed BHJ organic photovoltaic (OPV) devices. The best poly(3-hexylthiophene) (P3HT)/[6,6]-phenyl-C61-butyric acid methyl ester (PCBM) based bilayer structure OPV showed an external quantum efficiency approaching 82%, a high fill factor of 74%, and the power conversion efficiency of 5.1%, which are higher than those of the blend-solution-processed BHJ OPV devices. In contrast to the BHJ formed from blend solution, richer acceptor, e.g. PCBM, close to the cathode, or different morphology, was generally found in thermally annealed bilayer films. However, the physical mechanism for improved performance in thermally annealed bilayer films was rarely investigated in previous studies. Here, the amount of long-lived photogenerated charges with lifetime longer than 1 μs, which was characterized by the time delayed collection field method, was slightly enhanced by about 5% in the thermally annealed bilayer devices. Nevertheless, the bimolecular recombination coefficient was strongly decreased by 350% with transient photovoltage/photocurrent measurements, conclusively demonstrating that the significantly reduced bimolecular recombination loss is a major contribution to the increased efficiency in the thermally annealed bilayer OPVs.

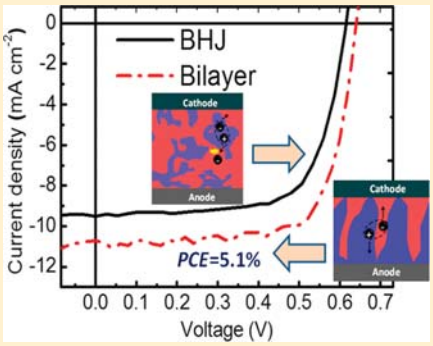

1. INTRODUCTION

Organic photovoltaics (OPVs) are promising candidates for clean and renewable energy harvesting due to their low cost, lightweight, flexibility, and high throughput fabrication capability. The power conversion efficiency (*PCE*) of OPVs has been quickly rising from ∼1% to above 10% in the past decade.[1] The first efficient OPV device was reported by C. Tang in 1986 which has a donor/acceptor bilayer structure fabricated by vacuum thermal evaporation deposition.[2] This record OPV device efficiency was not surmounted until the emergence of bulk heterojunction (BHJ) OPV designed by A. Heeger et. al in 1995.[3] In BHJ OPVs, mixtures of donors and acceptors were used as active layers to overcome the exciton diffusion bottleneck. The charge generation efficiency is dramatically improved by a very large interfacial area of donor and acceptor in BHJs and a much smaller donor/acceptor domain size which is within the diffusion length of Frenkel excitons[3] or the uncertain length of light.[4,5] Almost all recently reported OPVs with high *PCE* were based on the BHJ structure.[1,6−9]

Very recently, the feasibility to use a bilayer structure for highly efficient OPVs was revisited. It was first reported that the poly(3-hexylthiophene) (P3HT)/[6,6]-phenyl-C61-butyric acid methyl ester (PCBM) based bilayer structure OPVs, which were deposited by spin-coating using immiscible solvents for donor followed by thermal annealing, showed comparable performance to the optimized BHJ structure OPVs.[10] This bilayer structure was also applied to some other photovoltaic materials systems, yielding PCEs similar to those devices with a BHJ structure.[11] Interestingly, it was later found by several groups that the thermally annealed bilayer structure was actually a BHJ due to the interdiffusion of PCBM and P3HT.[12,13] The morphology of the BHJ formed by the interdiffusion was reported to be different from those formed by blend solution in that a richer PCBM close to the cathode was found in thermally annealed bilayer films.[12] However, the impact of the different morphology on charge generation and charge recombination in the thermally annealed bilayer structure OPVs and in BHJs was rarely discussed in previous studies. In this manuscript, we first show that the thermally annealed bilayer P3HT/PCBM OPV devices can be more efficient than the optimum BHJ counterparts, and the best bilayer device yielded an external quantum efficiency (*EQE*) approaching 82%, a fill factor (*FF*) of 74%, and a *PCE* of 5.1%; and then we systematically investigated the behind physical mechanism for improved performance in the thermally annealed bilayer OPVs by using a wide variety of independent characterization techniques.

Received: January 17, 2014
Revised: February 21, 2014
Published: February 24, 2014

   dx.doi.org/10.1021/jp500547j | *J. Phys. Chem. C* 2014, 118, 5196−5202

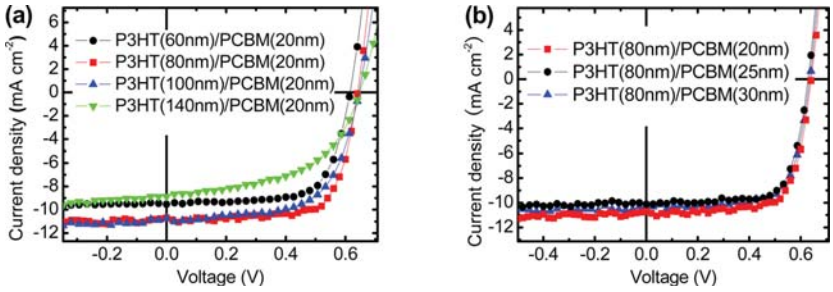

Figure 1. J-V curves of the P3HT/PCBM thermally annealed bilayer devices with different P3HT thickness (a) and different PCBM thickness (b).

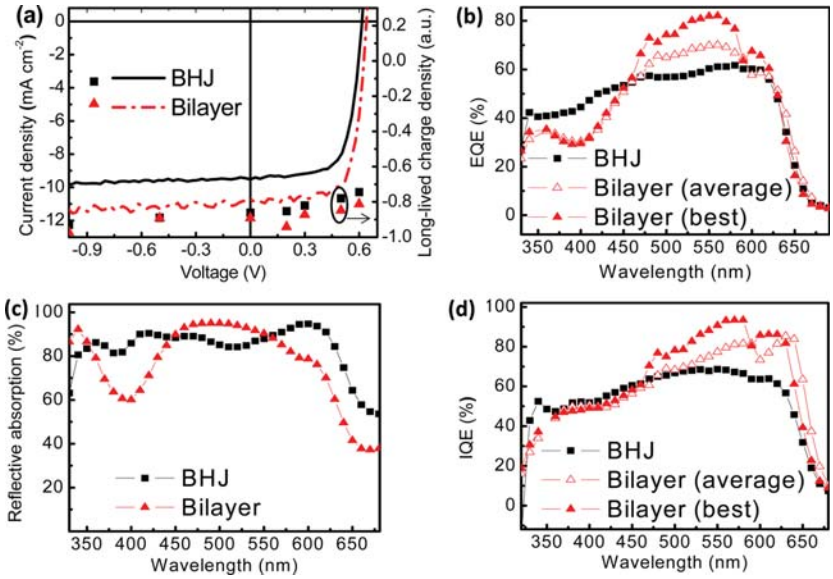

Figure 2. Comparison of device performance in BHJ and thermally annealed bilayer: (a) J-V curves under illumination of simulated AM 1.5G (100 mW cm^{-2}) and normalized long-lived photogenerated charge densities at various applied biases obtained by TDCF measurements, (b) EQE, (c) reflective absorption, and (d) IQE.

2. EXPERIMENTAL SECTION

The cleanness of indium tin oxide (ITO) glass and fabrication of subsequent poly(3,4-ethylenedioxythiophene):poly-(styrenesulfonate) (PEDOT:PSS) film followed the previous recipe.[1] The bilayer active films were prepared by following the reported method.[14] The P3HT (Rieke, used as received) solution, with concentration of 15 mg mL^{-1}, 20 mg mL^{-1}, or 30 mg mL^{-1}, was spin-coated onto PEDOT:PSS films. Subsequently, the P3HT films were baked at 50 °C for 5 min. The PCBM (Nano-C, used as received, 5 mg mL^{-1}), predissolved in dichloromethane, was then spin-coated onto the P3HT films with 350 rpm for 1 s followed by 4000 rpm for 10 s. Subsequently, the obtained bilayer P3HT/PCBM film was annealed at 150 °C for 20 min to drive the interdiffusion of PCBM into P3HT. The active films were covered by 20 nm calcium and 100 nm thick aluminum as cathode. The active device area is approximately 0.07 cm^2. Photocurrent was measured under irradiation of simulated AM 1.5G (100 mW cm^{-2}).

For the impedance spectroscopy measurement, the Agilent precision LCR meter E4980A (20 Hz-2 MHz) was connected in series to the device. The impedance spectroscopy of the device was measured under illumination intensity of 100 mW cm^{-2} and varied bias voltage (0−0.7 V). The applied bias was internally provided by the LCR meter E4980A. The photogenerated charge carrier lifetime under different applied bias voltage was fitted with the equivalent circuit model as shown in the inset of Figure 3c.

For the transient photocurrent/transient photovoltage (TPC/TPV) and differential capacitance experiment, the device was serially connected to a digital oscilloscope (LeCroy LT 342, with sampling rate of 500 Ms/s, bandwidth of 500 MHz), and the input impedance of the oscilloscope was 1 MΩ to form the open circuit condition for monitoring the charge decay dynamics. In order to change open circuit voltage (V_{OC}) and charge density in the device, a Newport Xe lamp was used as the background light illumination with broad range tunable light intensity. A strongly attenuated UV laser pulse (SRS NL 100 Nitrogen Laser) was used as a small perturbation to the background illumination on the device. The laser-pulse-induced photovoltage variation (ΔV) was smaller than 5% of the V_{OC} produced by the background illumination. The wavelength of the N_2 laser is 337 nm, the repeating frequency was ~10 HZ, and the pulse width was less than 3.5 ns. The amount of electric charge variation (ΔQ) was obtained by integrating short circuit current (J_{SC}) with time. The electrode capacitance charge density was subtracted from all the measured charge densities.

The dependence of the long-lived photogenerated charges on the applied bias was measured by the time delayed collection field (TDCF) method. The laser intensity of the N2

dx.doi.org/10.1021/jp500547j | J. Phys. Chem. C 2014, 118, 5196−5202

laser, with a shot-to-shot energy deviation of <3%, was attenuated by neutral density filters so that the photocurrent pulse height generated was comparable to the J_{SC}. An upgraded Keithley semiconductor parameter analyzer (4200-SCS) with two synchronized voltage output channels was used to trigger the nitrogen laser and provide charge collection bias, respectively. The rising time of the trigger pulse and the electrical bias pulse was 10 ns. The nitrogen laser provides a simultaneous TTL pulse output with a full width at half-maximum (fwhm) of 1 ns during the laser pulse output, enabling an accurate identification of the delay time between the laser pulse and charge extraction pulse. A digital oscilloscope with a bandwidth of 500 MHz was used to record the voltage pulse over a 50 Ω resistance which was connected in series with the device.

3. RESULTS AND DISCUSSION

The thicknesses of P3HT and PCBM layers were tuned to optimize the thermally annealed bilayer device performance. The first step was to change the P3HT thickness with a constant PCBM film thickness of 20 nm. As shown in Figure 1a, as the P3HT thickness increased from 60 to 80 nm, all the photovoltaic parameters showed a considerable enhancement. Nevertheless, further increasing the thickness of P3HT films, e.g. to 100 or 140 nm, deteriorated the device performance. The second step was to maintain the optimized P3HT film thickness at 80 nm and to vary the thickness of PCBM layer. It was observed that variation of the PCBM thickness from 20 to 30 nm did not alter the device performance too much as shown in Figure 1b, most likely because of the relatively small variation of PCBM thickness by the spin-coating method. The optimized thermally annealed bilayer OPVs showed average *PCE* of 4.6 ± 0.3%, average *FF* of 71 ± 2%, average V_{OC} of 0.64 ± 0.01 V, and average J_{SC} of 10.1 ± 0.2 mA cm^{-2} based on 11 devices, and the best device yielded a large V_{OC} of 0.64 V, a J_{SC} of 10.7 mA cm^{-2}, a *FF* of 74%, and a high *PCE* of 5.1% under illumination of simulated AM 1.5G (100 mW cm^{-2}).

To compare the performance of the BHJ and the thermally annealed bilayer devices, the optimized P3HT:PCBM BHJ devices with a blending ratio of 1:1 were fabricated using the previously established methods including solvent annealing[15] and thermal annealing.[16] The photocurrents of both types of devices under illumination of simulated AM 1.5G (100 mW cm^{-2}) are shown in Figure 2a. The P3HT:PCBM BHJ device produced a J_{SC} of 9.7 mA cm^{-2}, a V_{OC} of 0.61 V, a *FF* of 68%, and a *PCE* of around 4.0%, consistent with the previously reported value.[15] The efficiency of the thermally annealed P3HT/PCBM bilayer devices was around 28% larger than that of the BHJ counterparts. The *EQE* of these two types of devices are shown in Figure 2b. The BHJ device had a maximum *EQE* of about 62%, which is a typical value for P3HT:PCBM BHJ devices.[15] It is remarkable that the maximum *EQE* of the best thermally annealed bilayer OPV devices reached 82% at 560 nm, which was much larger than that of the BHJ devices. The average EQE curve was obtained based on 5 devices, and the maximum EQE was about 71 ± 13%, which was still higher than the BHJ devices as shown in Figure 2b. To our knowledge, this *EQE* value is among the highest reported ones of all the organic solar cells so far. The reflective absorption spectra were measured by using the same device. The internal quantum efficiency (*IQE*) was calculated by following the previous reported method.[17] We should note that our calculated *IQE* is the minimum *IQE* of the devices since the measured reflective absorption did not exclude the diffuse reflectance and parasitic absorption from the electrode at light incident side. As shown in Figure 2c, the reflective absorption of the bilayer films is slightly weaker than that of the BHJ films over almost the entire UV−visible range except between 450 nm and 550 nm. This can be explained by the much thinner active layer used in the bilayer devices (~85 nm) than in the BHJ devices (~150 nm). The smaller amount of PCBM in the thermally annealed bilayer devices than in the BHJ devices can also explain the lower *EQE* from 350 to 450 nm in the bilayer devices. As shown in Figure 2d, the calculated *IQE* of the thermally annealed bilayer devices is significantly larger than that of the BHJ devices at broad wavelength range from 500 to 650 nm. In particular, the maximum *IQE* in the thermally annealed bilayer device exceeds 90% at around 600 nm. The *IQE* is actually wavelength dependent, and the *IQE* is smaller at the shorter wavelength range where PCBM absorbs, explained by the too small exciton diffusion length (5 nm) in PCBM.[18] The wavelength dependence of the *IQE* at long wavelengths should be mainly due to unique internal morphology of the active film resulting in favorable domain size, charge collection, or optical interference for higher exciton harvesting efficiency in P3HT.[19] It is worth noting that this is the first time a significantly better device performance was achieved in thermally annealed bilayer devices than their BHJ counterparts.

It is interesting to understand the origin of the increased device performance in the thermally annealed bilayer devices. Since the *IQE* and device efficiency is strongly affected by the amount of photogenerated charges relative to the number of incident photons, we used the TDCF technique which can be used to characterize the long-lived photogenerated charges, whose recombination time scale is generally longer than 1 μs.[20,21] We compared the long-lived photogenerated charge densities at various applied biases in thermally annealed bilayer devices and their BHJ counterparts with using the same incident light intensity. A large reverse bias of −4 V with a delay time of 500 ns after the laser pulse (~337 nm) was used to sweep-out all the photogenerated long-lived charges. The transient photocurrent was obtained by subtracting the measured transient photocurrent under laser pulse with the capacitance discharge current measured in the dark. The photogenerated free charge densities at different applied biases were obtained by integrating the transient photocurrent over time. The long-lived photogenerated charge densities in thermally annealed bilayer OPV devices are relatively higher than that in the regular BHJ devices at the forward bias conditions. Therefore, the enhanced long-lived photogenerated charge density partially contributed to the increased device efficiency in the thermally annealed bilayer OPVs, which is most likely due to the morphology difference of the thermally annealed bilayer and BHJ films. It has been shown by T. Russel et al. that the thermally annealed bilayer finally evolves into a two-phase structure which involves a pure P3HT phase and a mixture of P3HT and PCBM phase.[12] The mixture phase was recently believed to play a critical role in the charge separation,[22−24] which explains the enhanced long-lived photogenerated charge density in the thermally annealed bilayer OPVs.

The small increase in long-lived photogenerated free charge densities cannot explain the significant increase of J_{SC}, and the weak field dependent long-lived photogenerated charge density cannot explain the greatly increased *FF* as shown in Figure 2a. The regular BHJs from blend solution generally contain dead

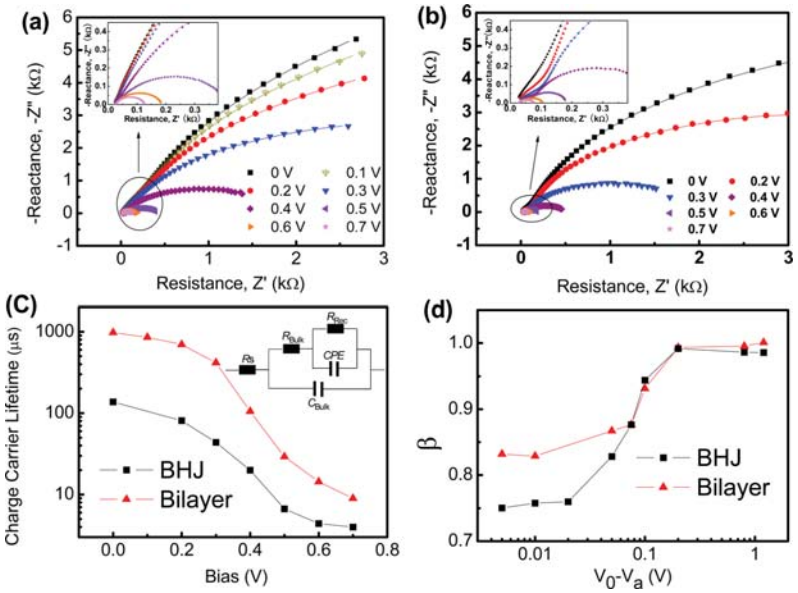

Figure 3. Impedance spectroscopy of thermally annealed bilayer (a) and BHJ (b) devices based on P3HT:PCBM; (c) Average charge carrier lifetime as a function of applied bias and the inset of (c) shows the fitting model of equivalent circuit; and (d) exponent β as a function of effective applied voltage V_o-V_a in thermally annealed bilayer and BHJ devices.

ends by the isolated donor or acceptor nanodomains which can impede the flow of charge carriers.[22] The free charge carriers generated or trapped in these isolated nanodomains are likely lost as heat by recombination.[25,26] Nevertheless, the BHJs from thermally annealed bilayer films structure are expected to have less dead ends than the regular BHJ films because the PCBM connects well along its diffusion paths. It is thus hypothesized that the thermally annealed bilayer devices would have weaker charge recombination loss than in the BHJ devices.

The charge recombination was evaluated in both types of devices with a variety of independent measurements. Impedance spectroscopy was shown to be a powerful method to characterize the average charge carrier lifetime (τ_{Ave}) in BHJ OPV devices.[27−29] Generally, the impedance spectroscopy is calculated by dividing an applied sinusoidal voltage by the output sinusoidal current. In our measurement, the amplitude of 10 meV of the applied sinusoidal voltage bias was utilized. The impedance spectroscopy is frequency dependent, and its imaginary part and real part is reactance and resistance, respectively, as shown in Figure 3a-b. The impedance spectroscopy characterization reveals essential information on charge carrier transport and recombination in organic solar cells. A few of the different equivalent circuit models have been proposed for different research purposes, e.g., revealing the trap-assisted recombination in organic solar cells,[29] characterizing the bimolecular recombination at the donor/acceptor interfaces,[28] and revealing the charge carrier mobility in the bulk active films.[27] The used circuit model in our manuscript was referred from a good work by Leever et al.,[28] which was proposed to reveal the bimolecular recombination at the donor/acceptor interfaces by characterizing the effective charge carrier lifetime difference in terms of morphological variation in P3HT:PCBM films. For the same purpose, we referred this equivalent circuit model to characterize the charge carrier lifetime in terms of morphology differences in our P3HT/PCBM active film based BHJ and thermally annealed bilayer devices. The Cole−Cole plots in the BHJ and thermally annealed bilayer devices were measured under illumination of simulated AM 1.5G with applied forward bias ranging from 0 to 0.7 V, and the results were shown in Figure 3a-b. The data was fitted with the equivalent circuit model (inset of Figure 3c) as reported elsewhere.[28]

Why is the used equivalent circuit model appropriate for our measured impedance data in P3HT/PCBM based devices? First of all, since an organic solar cell is composed of a donor/acceptor blend layer sandwiched between an anode and a cathode, a parallel circuit of resistor (R) - capacitor (C) is expected, where C represents a bulk capacitor (C_{Bulk}), and R comes from two parts: one is bulk resistance (R_{Bulk}) from an active layer itself such as P3HT/PCBM based active film in our devices, the other is recombination resistance (R_{Rec}) from the recombination of photogenerated electrons and holes. Since these photogenerated electrons and holes normally reside on acceptors and donors, respectively, a chemical capacitor is resulted in.[29] In order to account for inhomogeneous morphological distribution, the constant phase element (C_{CPE}) instead of a chemical capacitor is used in our fitting model. A parallel circuit of R_{Rec} and C_{CPE} is used to account for photogenerated electrons and holes in the active layer. Finally, since the serial resistance from electrodes and electrode/active layer-interface contact is commonly seen in organic solar cells, a serial resistor (Rs) is serially connected with the whole R-C circuit in our circuit model. Since the two parameters, R_{Rec} and C_{CPE}, are related to the bimolecular recombination of electrons on acceptors and holes on donors in the active films, τ_{Ave} can be determined according to the following equation:[28,29]

$$\tau_{Ave} = R_{Rec} \cdot C_{CPE} \quad (1)$$

Figure 3c shows that the τ_{Ave} in the thermally annealed bilayer devices is apparently longer than that in the BHJ devices at various applied biases ranging from 0 to 0.7 V, which demonstrates that the bimolecular recombination loss in thermally annealed bilayer OPVs is much weaker than that in the BHJ OPVs. In both types of devices, the τ_{Ave} decreases with bias from 0 to 0.7 V. This can be understood by the fact that the τ_{Ave} reduces with increasing charge carrier density which is

dx.doi.org/10.1021/jp500547j | J. Phys. Chem. C 2014, 118, 5196−5202

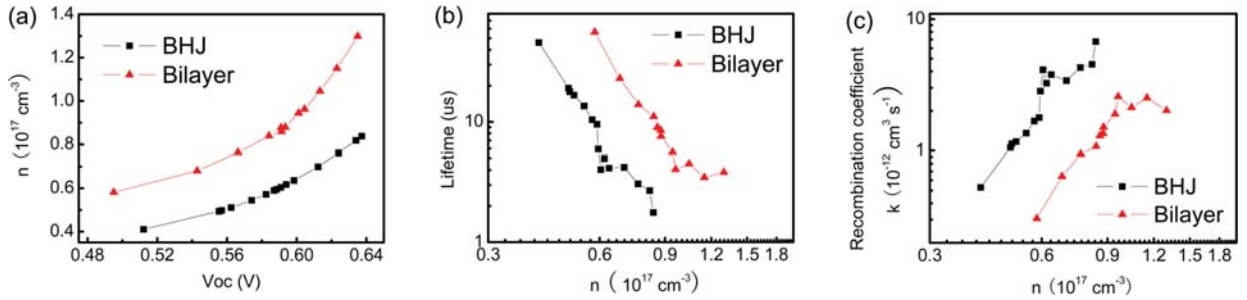

Figure 4. (a) The obtained charge carrier density (n) as a function of V_{OC}, (b) variation of carrier lifetime with charge density, and (c) the calculated bimolecular recombination coefficient as a function of carrier density in the BHJ and thermally annealed bilayer devices.

caused by the stronger charge injection at larger forward bias and less efficient charge extraction with the reduced effective built-in electric field.

Previous studies concluded that the bimolecular recombination is the dominating recombination loss mechanism at open circuit condition in the P3HT:PCBM BHJ OPVs.[25,26,29,30] In order to qualify and quantify the bimolecular recombination difference in the thermally annealed bilayer and the BHJ OPVs, two independent measurements were conducted here: a light intensity dependent steady-state photocurrent and transient photovoltage/photocurrent characterization. For the light intensity dependence study,[29,30] the effective photocurrents (J_{ph}) under light intensity (I) from 1 mW cm^{-2} to 100 mW cm^{-2} were obtained from subtracting the measured photocurrents (J) under different light intensity with the dark current (J_d). The recombination parameter beta (β) is obtained by fitting $J_{ph} \approx I^{\beta}$. It should be noted that a larger β conclusively reflects less bimolecular recombination in the devices despite the fact that it is still under debate on how to derive the percentage of recombination type from the recombination parameter β.[29,30] Figure 3d shows the fitting exponent β as a function of effective applied voltage (V_0−V), where V_0 is the effective V_{OC} at J_{ph} = 0 and V is the applied voltage bias. It is clear that the thermally annealed bilayer OPVs have weaker bimolecular recombination than the BHJ OPVs at applied bias close to V_{OC}.

In order to further quantify the bimolecular charge recombination dynamics difference between the thermally annealed bilayer OPVs and regular BHJ OPVs, the TPV/TPC measurement has been conducted. For the TPV measurement, the device was connected in series with a digital oscilloscope whose input impedance was set to 1 MΩ to form the open circuit condition for monitoring the charge decay dynamics. A strong tunable background light continuously illuminates the device to tune the total population of charge density in the device, and a strongly attenuated UV laser pulse was simultaneously used as a small perturbation in the device. It is noted that the laser-pulse-induced ΔV should be smaller than 5% of the V_{OC} generated by the background illumination. The decay kinetics of small perturbation charges, which is generated by the applied pulse laser, can be described with the following equation[26,31,32]

$$\frac{d\Delta n}{dt} = -\alpha\frac{\Delta n}{\tau} \tag{2}$$

where α is the recombination order, which means eq 2 describes first-order recombination if α equals 1, whereas eq 2 describes second-order recombination if α equals 2; Δn is the perturbation charge density; and τ is the charge carrier lifetime. The charge lifetime was obtained from the TPV measurements by fitting the second-order charge decay kinetics by using eq 2, where α equals 2. For the TPC measurement, a device was connected in series with a 10 Ω resistor, over which the laser-pulsed-induced charge decay dynamics was recorded with a digital oscilloscope. By combining TPV and TPC, a differential capacitance technique was used to analyze the steady-state charge carrier density under illumination of various background light intensities at open circuit condition.[26,31,32] The obtained charge carrier density as a function of V_{OC} is plotted in Figure 4a, where the V_{OC} was tuned through varying the background illumination intensity. The charge density in thermally annealed bilayer OPV is larger than in the regular BHJ OPV at any given V_{OC}, which could be due to the enhanced photogenerated charge density as shown by TDCF measurement and/or suppressed charge recombination. The carrier density dependent carrier lifetime is shown in Figure 4b, which is consistent with our above-mentioned bias dependent lifetime data obtained from impedance spectroscopy method (Figure 3c). The higher charge density at larger bias voltage undoubtedly leads to smaller carrier lifetime. The carrier lifetime in BHJs is comparable to the reported value,[31] while carrier lifetime in the bilayer devices is significantly longer than in the regular BHJ devices at any given charge carrier concentrations. Since the bimolecular recombination dominates at the V_{OC} conditions in the P3HT:PCBM material system, the total population of charges decay dynamics is described as the following bimolecular recombination kinetic equation[26]

$$\frac{dn}{dt} = -kn^2 \tag{3}$$

where n is the photogenerated charges, and k is the bimolecular recombination coefficient. The bimolecular recombination coefficient k at any given carrier concentration n can be derived from eq 3[26,31]

$$k = \frac{1}{\tau(n)\cdot n} \tag{4}$$

where $\tau(n)$ is the carrier lifetime at the given carrier concentration. The calculated bimolecular recombination coefficient as a function of carrier concentration is shown in Figure 4c. It is clear that the bimolecular recombination coefficient of the bilayer OPV device is around 350% smaller than that of blend-solution-processed BHJ OPV device. The much smaller bimolecular recombination coefficient agrees with the expectation that a better connected interpenetrating P3HT:PCBM film formed by a thermally annealed bilayer film should reduce the bimolecular charge recombination loss by avoiding the formation of dead ends. In addition, it has been

dx.doi.org/10.1021/jp500547j | J. Phys. Chem. C 2014, 118, 5196−5202

shown that a PCBM rich thin layer is close to the cathode side and a P3HT rich layer is close to the anode side in the thermally annealed bilayer films.[12] The charge recombination at anode/PCBM and cathode/P3HT is thus reduced in the thermally annealed bilayer OPVs, which should also contribute to the increased charge carrier lifetime observed here.

4. CONCLUSIONS

In summary, the highest reported *PCE* of 5.1% for the P3HT:PCBM system was demonstrated in the thermally annealed bilayer OPVs which showed a high *EQE* of 82%, *FF* of 74%, and *IQE* of around 90%. The bilayer structure has been shown to yield superior device performance to the currently popular BHJ structure most likely due to the better bicontinuous donor/acceptor internal morphology, which leads to strongly reduced bimolecular recombination.

AUTHOR INFORMATION

Corresponding Author

*E-mail: jhuang2@unl.edu.

Notes

The authors declare no competing financial interest.

ACKNOWLEDGMENTS

We thank the financial support by the National Science Foundation under Awards ECCS-1201384 and ECCS-1252623, and the Nebraska Public Power District through the Nebraska Center for Energy Sciences Research.

REFERENCES

(1) You, J.; Dou, L.; Yoshimura, K.; Kato, T.; Ohya, K.; Moriarty, T.; Emery, K.; Chen, C.-C.; Gao, J.; Li, G. A Polymer Tandem Solar Cell with 10.6% Power Conversion Efficiency. *Nat. Commun.* **2013**, *4*, 1446.

(2) Tang, C. W. Two-Layer Organic Photovoltaic Cell. *Appl. Phys. Lett.* **1986**, *48*, 183.

(3) Yu, G.; Gao, J.; Hummelen, J.; Wudl, F.; Heeger, A. Polymer Photovoltaic Cells: Enhanced Efficiencies via a Network of Internal Donor-Acceptor Heterojunctions. *Science* **1995**, *270*, 1789−1791.

(4) Kaake, L. G.; Jasieniak, J. J.; Bakus, R. C.; Welch, G. C.; Moses, D.; Bazan, G. C.; Heeger, A. J. Photoinduced Charge Generation in a Molecular Bulk Heterojunction Material. *J. Am. Chem. Soc.* **2012**, *134*, 19828−19838.

(5) Kaake, L. G.; Moses, D.; Heeger, A. J. Coherence and Uncertainty in Nanostructured Organic Photovoltaics. *J. Phys. Chem. Lett.* **2013**, *4*, 2264−2268.

(6) Chen, H.-Y.; Hou, J.; Zhang, S.; Liang, Y.; Yang, G.; Yang, Y.; Yu, L.; Wu, Y.; Li, G. Polymer Solar Cells with Enhanced Open-Circuit Voltage and Efficiency. *Nat. Photonics* **2009**, *3*, 649−653.

(7) Hoke, E. T.; Vandewal, K.; Bartelt, J. A.; Mateker, W. R.; Douglas, J. D.; Noriega, R.; Graham, K. R.; Fréchet, J. M. J.; Salleo, A.; McGehee, M. D. Recombination in Polymer: Fullerene Solar Cells with Open-Circuit Voltages Approaching and Exceeding 1.0 V. *Adv. Energy Mater.* **2012**, *3*, 220−230.

(8) Sista, S.; Park, M. H.; Hong, Z.; Wu, Y.; Hou, J.; Kwan, W. L.; Li, G.; Yang, Y. Highly Efficient Tandem Polymer Photovoltaic Cells. *Adv. Mater.* **2010**, *22*, 380−383.

(9) Small, C. E.; Chen, S.; Subbiah, J.; Amb, C. M.; Tsang, S.-W.; Lai, T.-H.; Reynolds, J. R.; So, F. High-Efficiency Inverted Dithienogermole-Thienopyrrolodione-Based Polymer Solar Cells. *Nat. Photonics* **2011**, *6*, 115−120.

(10) Ayzner, A. L.; Tassone, C. J.; Tolbert, S. H.; Schwartz, B. J. Reappraising the Need for Bulk Heterojunctions in Polymer−Fullerene Photovoltaics: the Role of Carrier Transport in All-Solution-Processed P3HT/PCBM Bilayer Solar Cells. *J. Phys. Chem. C* **2009**, *113*, 20050−20060.

(11) Huang, J.-H.; Li, K.-C.; Kekuda, D.; Padhy, H. H.; Lin, H.-C.; Ho, K.-C.; Chu, C.-W. Efficient Bilayer Polymer Solar Cells Possessing Planar Mixed-Heterojunction Structures. *J. Mater. Chem.* **2010**, *20*, 3295−3300.

(12) Chen, D.; Liu, F.; Wang, C.; Nakahara, A.; Russell, T. P. Bulk Heterojunction Photovoltaic Active Layers via Bilayer Interdiffusion. *Nano Lett.* **2011**, *11*, 2071−2078.

(13) Moon, J. S.; Takacs, C. J.; Sun, Y.; Heeger, A. J. Spontaneous Formation of Bulk Heterojunction Nanostructures: Multiple Routes to Equivalent Morphologies. *Nano Lett.* **2011**, *11*, 1036−1039.

(14) Lee, K. H.; Schwenn, P. E.; Smith, A. R.; Cavaye, H.; Shaw, P. E.; James, M.; Krueger, K. B.; Gentle, I. R.; Meredith, P.; Burn, P. L. Morphology of All-Solution-Processed "Bilayer" Organic Solar Cells. *Adv. Mater.* **2011**, *23*, 766−770.

(15) Li, G.; Shrotriya, V.; Huang, J.; Yao, Y.; Moriarty, T.; Emery, K.; Yang, Y. High-Efficiency Solution Processable Polymer Photovoltaic Cells by Self-Organization of Polymer Blends. *Nat. Mater.* **2005**, *4*, 864−868.

(16) Ma, W.; Yang, C.; Gong, X.; Lee, K.; Heeger, A. J. Thermally Stable, Efficient Polymer Solar Cells with Nanoscale Control of the Interpenetrating Network Morphology. *Adv. Funct. Mater.* **2005**, *15*, 1617−1622.

(17) Huang, J.; Yang, Y. Origin of Photomultiplication in C60 Based Devices. *Appl. Phys. Lett.* **2007**, *91*, 203505.

(18) Cook, S.; Furube, A.; Katoh, R.; Han, L. Estimate of Singlet Diffusion Lengths in PCBM Films by Time-Resolved Emission Studies. *Chem. Phys. Lett.* **2009**, *478*, 33−36.

(19) Burkhard, G. F.; Hoke, E. T.; Scully, S. R.; McGehee, M. D. Incomplete Exciton Harvesting from Fullerenes in Bulk Heterojunction Solar Cells. *Nano Lett.* **2009**, *9*, 4037−4041.

(20) Kniepert, J.; Schubert, M.; Blakesley, J. C.; Neher, D. Photogeneration and Recombination in P3HT/PCBM Solar Cells Probed by Time-Delayed Collection Field Experiments. *J. Phys. Chem. Lett.* **2011**, *2*, 700−705.

(21) Offermans, T.; Meskers, S. C.; Janssen, R. A. Time Delayed Collection Field Experiments on Polymer: Fullerene Bulk-Heterojunction Solar Cells. *J. Appl. Phys.* **2006**, *100*, 074509.

(22) Bartelt, J. A.; Beiley, Z. M.; Hoke, E. T.; Mateker, W. R.; Douglas, J. D.; Collins, B. A.; Tumbleston, J. R.; Graham, K. R.; Amassian, A.; Ade, H.; Fréchet, J. M. J.; Toney, M. F.; McGehee, M. D. The Importance of Fullerene Percolation in the Mixed Regions of Polymer−Fullerene Bulk Heterojunction Solar Cells. *Adv. Energy Mater.* **2013**, *3*, 364−374.

(23) Liu, T.; Cheung, D. L.; Troisi, A. Structural Variability and Dynamics of the P3HT/PCBM Interface and its Effects on the Electronic Structure and the Charge-Transfer Rates in Solar Cells. *Phys. Chem. Chem. Phys.* **2011**, *13*, 21461−21470.

(24) McMahon, D. P.; Cheung, D. L.; Troisi, A. Why Holes and Electrons Separate So Well in Polymer/Fullerene Photovoltaic Cells. *J. Phys. Chem. Lett.* **2011**, *2*, 2737−2741.

(25) Cowan, S. R.; Roy, A.; Heeger, A. J. Recombination in Polymer-Fullerene Bulk Heterojunction Solar Cells. *Phys. Rev. B* **2010**, *82*, 245207.

(26) Shuttle, C.; O'Regan, B.; Ballantyne, A.; Nelson, J.; Bradley, D.; Durrant, J. Bimolecular Recombination Losses in Polythiophene: Fullerene Solar Cells. *Phys. Rev. B* **2008**, *78*, 113201.

(27) Garcia-Belmonte, G.; Munar, A.; Barea, E. M.; Bisquert, J.; Ugarte, I.; Pacios, R. Charge Carrier Mobility and Lifetime of Organic Bulk Heterojunctions Analyzed by Impedance Spectroscopy. *Org. Electron.* **2008**, *9*, 847−851.

(28) Leever, B. J.; Bailey, C. A.; Marks, T. J.; Hersam, M. C.; Durstock, M. F. In Situ Characterization of Lifetime and Morphology in Operating Bulk Heterojunction Organic Photovoltaic Devices by Impedance Spectroscopy. *Adv. Energy Mater.* **2012**, *2*, 120−128.

(29) Leong, W. L.; Cowan, S. R.; Heeger, A. J. Differential Resistance Analysis of Charge Carrier Losses in Organic Bulk Heterojunction Solar Cells: Observing the Transition from Bimolecular to Trap-

Assisted Recombination and Quantifying the Order of Recombination. *Adv. Energy Mater.* **2011**, *1*, 517−522.
(30) Koster, L.; Mihailetchi, V.; Blom, P. Bimolecular Recombination in Polymer/Fullerene Bulk Heterojunction Solar Cells. *Appl. Phys. Lett.* **2006**, *88*, 052104.
(31) Hamilton, R.; Shuttle, C. G.; O'Regan, B.; Hammant, T. C.; Nelson, J.; Durrant, J. R. Recombination in Annealed and Non-annealed Polythiophene/Fullerene Solar Cells: Transient Photovoltage Studies Versus Numerical Modeling. *J. Phys. Chem. Lett.* **2010**, *1*, 1432−1436.
(32) Shuttle, C.; ORegan, B.; Ballantyne, A.; Nelson, J.; Bradley, D.; De Mello, J.; Durrant, J. Experimental Determination of the Rate Law for Charge Carrier Decay in a Polythiophene: Fullerene Solar Cell. *Appl. Phys. Lett.* **2008**, *92*, 093311.